# Assessment of the Statistical Characterization of Small-Scale Rainfall Variability from Radar: Analysis of TRMM Ground Validation Datasets

MEKONNEN GEBREMICHAEL AND WITOLD F. KRAJEWSKI

*IIHR-Hydroscience and Engineering, The University of Iowa, Iowa City, Iowa*

(Manuscript received 18 July 2003, in final form 20 February 2004)

ABSTRACT

The main objective of this study is to assess the ability of radar-derived rainfall products to characterize the small-scale spatial variability of rainfall. The authors use independent datasets from high-quality dense rain gauge networks employed during the Texas and Florida Underflights (TEFLUN-B) and Tropical Rainfall Measuring Mission component of the Large-Scale Biosphere–Atmosphere (TRMM-LBA) field experiments conducted by NASA in 1998 and 1999. A detailed comparison between gauge- and radar-derived spatial variability estimates is carried out by means of a correlation function, covariance, variogram, scaling characteristics, and variance reduction due to spatial averaging. Emphasis is given to the correlation function because it is involved in most of these statistics. The approach followed in the analysis addresses the problems associated with the traditional estimation methods and the recognized differences in the scales of observation. The performance of the radar-derived correlation function is evaluated in two ways: by direct comparison with gauge-derived correlation function and by quantifying its effect on one of the applications, that is, gauge sampling uncertainty estimation. Results show that, at separation distances shorter than about 5 km, radar-derived correlations are lower than those obtained from gauges. Three sources of uncertainty that may have caused the discrepancy between gauge- and radar-derived correlations are identified, and their effects are quantified to the extent possible. The error introduced in gauge sampling uncertainty estimates due to the use of radar-derived correlation function is within 30%. Discrepancies between gauge- and radar-rainfall fields are also observed in terms of the other spatial statistics.

## 1. Introduction

A high-quality dense rain gauge network is ideally required to capture the small-scale rainfall variability. In the absence of such a network, ground-based radar data are increasingly used to estimate the small-scale rainfall variability (Zawadzki 1973; Seed and Austin 1990; Pereira Fo and Crawford 1999; Moszkowicz 2000; Germann and Joss 2001; Datta et al. 2003). However, despite their potential to give spatial patterns, radars are known to have limitations. Radar-derived rainfall estimates are subject to a number of error sources, including natural variability of drop size distribution, variation of reflectivity with height, attenuation of radar signal, and radar hardware miscalibration and noise (e.g., Austin 1987; Joss and Waldvogel 1990; Smith and Krajewski 1993; Joss and Lee 1995). Krajewski et al. (1996) showed through a simulation experiment how difficult it is to retrieve the statistical properties of the true rain fields from the reflectivity fields. Also, radar-derived rainfall estimates are given as an average value over an area (i.e., the spatial resolution, usually 2 km $\times$ 2 km), and it is difficult to relate the rainfall variability at the scale of this resolution to smaller-scale rainfall variability. Because of these limitations, it is important to assess the accuracy of radar-derived spatial variability estimates.

Information about the small-scale (less than $\sim$20 km) variability of rainfall is essential in many theoretical and practical applications. One of the applications involves quantitative assessment of remote sensing rainfall products. Such products, which are available at a resolution of a few kilometers, are often compared with gauge point measurements for validation. Inferences about the rain rate around the gauge depend on the degree of spatial variability, which varies in time and space and as a function of the integration time.

Barnston (1991) and Ciach and Krajewski (1999a) proposed a method for estimating the radar-rainfall error variance, assuming that radar–gauge differences can be partitioned into the error of the radar estimate and the gauge sampling error. To estimate the second component, the spatial correlation function is required at scales below the size of the radar pixel. For example, Habib and Krajewski (2002) showed that for a correlation distance of about 5 km, the ratio of radar error variance

*Corresponding author address:* Witold F. Krajewski, IIHR-Hydroscience and Engineering, The University of Iowa, Iowa City, IA 52242-1585.
E-mail: witold-krajewski@uiowa.edu

to the total radar–gauge difference variance is of the order of 20%–60%. In a recent study, Gebremichael et al. (2003) applied this method successfully to obtain the error variance of satellite-derived rainfall products.

Another application involves estimating the number of satellite visits needed to identify the bias in satellite-rainfall algorithms. Several studies addressed this issue using stochastic models that require the spatial correlation function (North and Nakamoto 1989; Valdes et al. 1994; Yoo et al. 1996; Ha and North 1999; Bell and Kundu 2003). For example, Ha and North (1999) reported that for a field-of-view width of 20 km and a correlation length of a few kilometers, the number of satellite–gauge pairs (containing rain) necessary to distinguish a bias of 10% is on the order of 100. Other applications in which the small-scale spatial variability of rainfall is required include the design of ground validation schemes for remote sensing rainfall products (Ha and North 1999), merging radar-rainfall and rain gauge data using statistical methods (Krajewski 1987), the simulation of cloud fields in the estimation of rainfall from satellite passive microwave radiometers (Kummerow et al. 1996), storm movements and velocities (Niemczynowicz 1988), rainfall-runoff modeling (Winchell et al. 1998), and estimation of attenuation in communications (Capsoni et al. 1987).

The objective of our study is to assess how well the statistics of small-scale spatial variability of rainfall are captured by ground-based radars. We performed the assessment by comparing radar-derived spatial structures with the corresponding estimates obtained from a high-quality dense rain gauge network. The underlying premise of this study is that discrepancies between radar- and gauge-derived spatial variability estimates are mainly attributed to uncertainties in radar-derived estimates. This premise is reasonable because the instrumental and spatial representativeness errors, which are the most important error sources of gauge rainfall, are greatly minimized in high-quality dense rain gauge networks, such as those used in this study. We used a suite of statistical techniques to characterize the spatial structure of rainfall. To be specific, we compared the gauge- and radar-rainfall fields through their respective correlation function, covariance, variogram, scaling characteristics, and variance reduction due to spatial averaging. These characteristics have conceptually accessible physical interpretations, allowing for an understanding of the spatial structure of the fields from different perspectives.

We used surface rainfall observations collected during two of the National Aeronautics and Space Administration (NASA)'s Tropical Rainfall Measuring Mission (TRMM) field experiments: the Texas and Florida Underflights (TEFLUN-B) and the TRMM Large-Scale Biosphere–Atmosphere (TRMM-LBA) experiment. We describe the rainfall products and the regions of interest in the next section. In sections 3 and 4, we discuss the analysis method and implementation issues. Results are presented and discussed in section 5. This is followed by an application-based evaluation of radar-derived statistics in section 6. We close the paper with conclusions in section 7.

## 2. Experimental data and regions of interest

The data used in this study were collected by rain gauge networks and ground-based radars deployed during two TRMM campaigns: TEFLUN-B, which was conducted from 1 August through 27 September 1998 and focused on central Florida, and TRMM-LBA, which took place in the southwest of the Amazon basin from 10 January through 28 February 1999.

The rain gauge networks at both experimental sites consisted of tipping-bucket gauges with a volume resolution of 0.25 mm. The gauges were connected to dataloggers that were set to sampling resolutions of 5–10 s. Using a linear interpolation scheme (Habib et al. 2001b), we converted the raw rain gauge data into estimates of 1-min rain rates. Despite frequent maintenance visits to the gauges during the field campaigns, there were technical problems that hinder data collection. Debris in the gauge orifice and moisture condensation, causing short-circuits, were among the most typical problems encountered. We performed a quality control of the collected gauge observations using closely located gauges and the dual-gauge setup at some sites. We identified possible malfunctioning periods of gauge observations by analyzing 1) double-mass curves of rainfall amounts of dual gauges and pairs of gauges that were close to each other, and 2) the behavior of some spatial statistics, such as variation of correlation coefficients with intergauge distances. For the closely located gauges or dual-gauge setups, quality control was easier and resulted in much-improved data. Our confidence in the data quality was lower for some of the gauges that did not have other gauges nearby. We believe that the data quality problems that may have escaped our quality control analysis do not significantly affect the outcome of this study.

The Weather Surveillance Radar-1988 Doppler (WSR-88D) was operational during TEFLUN-B, and the National Center for Atmospheric Research (NCAR) S-band dual-polarization Doppler radar (S-POL) was used during TRMM-LBA. Both TEFLUN-B and TRMM-LBA were characterized by localized short-lived and intense convective cells typical of such tropical environments. The Atlantic Ocean fully occupies northeast and southeast quadrants of the TEFLUN-B radar domain. The summer rainfall in central Florida is influenced, to a large extent, by sea-breeze convection. In contrast, the Amazon basin is located thousands of kilometers from the ocean and there are no constant winds to drive the moisture ashore. The moisture is largely provided by the tropical rainforest trees (Petersen et al. 2002). Details of the rainfall products and the regions of interest are given below.

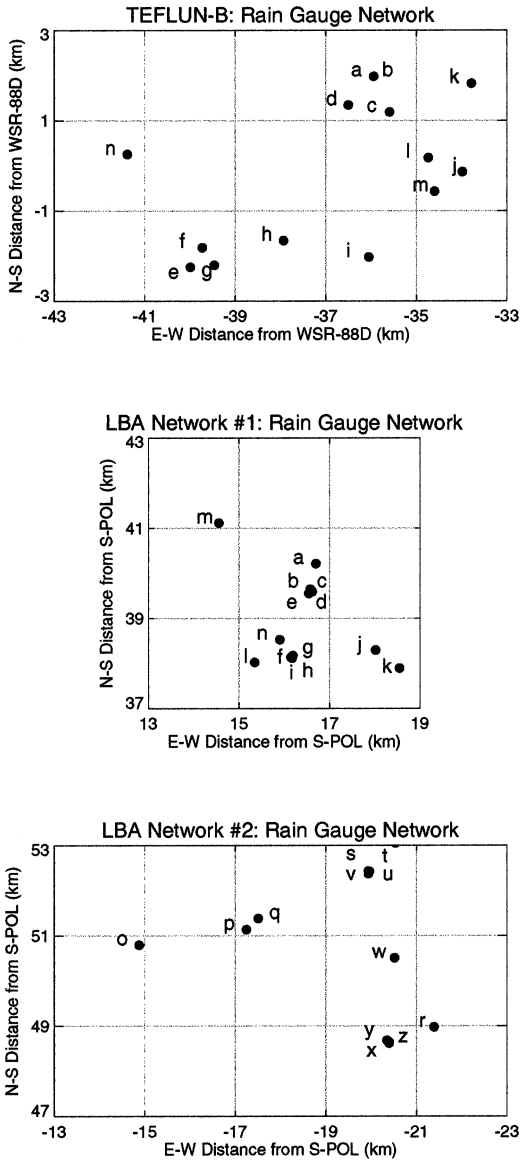


FIG. 1. Diagram of rain gauge networks deployed during TEFLUN-B and TRMM-LBA field experiments. The 2 km × 2 km grids represent the Cartesian pixels of the radar-rainfall maps. Each gauge is labeled with an identifier letter for the purpose of this study (see Tables 6 and 7 later for the correspondence between letter and official identification number).

### *a. TEFLUN-B*

The radar-rainfall products evaluated for TEFLUN-B are the standard 2A53 products provided by the TRMM Ground Validation Program (GVP). These products are generally available at a square pixel size of 2 km, covering an area of 300 km × 300 km, with a temporal frequency of ~5 min. The 2A53 products represent ''instantaneous'' rainfall rates constructed from radar volume scans collected by the Melbourne, Australia, WSR-88D. In deriving 2A53 products from radar reflectivities, the GVP team implemented the following procedure: (i) estimate rain rate using the relation $Z = AR^b$, with $A = 300$ and $b = 1.4$; (ii) compare the convective and stratiform monthly accumulations to gauge accumulations; and (iii) adjust the coefficient $A$ (while keeping the exponent $b$ as 1.4) to force agreement between radar and gauge data. The gauge network used in this study was not involved in the derivation of 2A53, and so it can be considered as an independent source of data. Detailed information can be found in Heiss et al. (1990) and Crum et al. (1993) regarding the characteristics of WSR-88D and in Marks et al. (2000) and Robinson et al. (2000) regarding the algorithms involved in deriving 2A53.

### *b. TRMM-LBA*

The radar-rainfall products evaluated for TRMM-LBA were derived using the differential phase method of Ryzhkov et al. (2000) by the Colorado State University Radar Meteorology Group. Rain gauge data were not involved in the derivation of these products. Although the rainfall maps were available approximately every 10 min for the experimental period, around-the-clock S-POL operations began on 16 January 1999. The rain maps are available at a square pixel size of 2 km covering an area of 200 km × 200 km. A description of the scanning strategy, the parameters collected by the radar, and the phase-based rainfall estimation technique can be found in Ryzhkov et al. (2000) and Cifelli et al. (2002).

### *c. Regions of interest*

Because we are interested in the direct comparison of gauge- and radar-derived statistics, we defined our region of interest as a subset of the radar map that is centered over the gauge network. This region includes the radar pixels containing gauges and the intervening pixels as well. Figure 1 depicts the selected regions of interest, the layout of gauge networks with respect to square grids of 2 km (radar-rainfall resolution), and distances from the radar center. The radars are located at (28.113°N, 80.654°W) in TEFLUN-B and at (11.222°S, 61.997°W) in TRMM-LBA. For TEFLUN-B, the selected region has an area of 6 km × 10 km (Fig. 1 top). The corresponding gauge network consisted of 14 gauges. The longest intergauge distance was 7.8 km.

For TRMM-LBA, our region of interest is a combination of a 6 km × 6 km area centered over network 1 and a 6 km × 10 km area centered over network 2. Networks 1 and 2 were spaced about 35 km apart, each containing 14 and 13 gauges. We rejected two of these gauges because they were often malfunctioning. The longest intergauge distance covered by these networks was 4.7 km.

## 3. Methods of analysis

We carried out the analysis in the framework of the theory of random functions (Vanmarcke 1983). The probabilistic quantities typically employed to characterize the spatial variability of rainfall are the first and second moments of a marginal probability distribution and the parameters of a spatial correlation function. Some degree of stationarity assumption is usually made to obtain solutions. In the simplest case this amounts to assuming that the probabilistic quantities mentioned above are uniform over the region of interest. We used a suite of statistical analysis: correlation function, variance reduction due to spatial averaging, covariance, variogram, and scaling characteristics. In this section, we describe each method and give its physical interpretation.

### a. Correlation estimation

Let the rainfall process $R(x, y)$ be the random process field, with $R$ as the rainfall intensity at location $(x, y)$. The linear dependence between the values assumed by $R(x, y)$ at two locations $(x_1, y_1)$ and $(x_2, y_2)$ separated by the lag $h$, where $h$ is the Euclidean distance between the points $(x_1, y_1)$ and $(x_2, y_2)$, can be represented by the correlation defined as

$$\rho(h) = \frac{E\langle\{R(x_1, y_1) - E[R(x_1, y_1)]\}\{R(x_2, y_2) - E[R(x_2, y_2)]\}\rangle}{\sqrt{\mathrm{Var}[R(x_1, y_1)]\mathrm{Var}[R(x_2, y_2)]}}, \quad (1)$$

where $E[\ ]$ and $\mathrm{Var}[\ ]$ are the expectation and variance operators, respectively. Equation (1) assumes that $\rho(h)$ depends on lag $h$ only and not on the position $(x, y)$. This assumption seems reasonable given the fact that our region of interest is small in size and the topography is nearly flat. The attractive feature of correlation is that it represents in a nondimensional form the intensity of the linear relationship between $R(x_1, y_1)$ and $R(x_2, y_2)$, enabling the direct comparison of the intensity of the relationship at different pairs of points. The popular estimator of (1) is the Pearson's product moment sample correlation,

$$r(h) = \frac{\langle R(x_1, y_1)R(x_2, y_2)\rangle - \langle R(x_1, y_1)\rangle\langle R(x_2, y_2)\rangle}{\sqrt{[\langle R(x_1, y_1)^2\rangle - \langle R(x_1, y_1)\rangle^2][\langle R(x_2, y_2)^2\rangle - \langle R(x_2, y_2)\rangle^2]}}, \quad (2)$$

where the angular brackets $\langle\ \rangle$ indicate the sample average.

There are concerns that need to be addressed in the application of the correlation function. It has been argued that the estimator (2) shows little robustness with respect to data nonnormality (e.g., Kowalski 1972). For data with lognormal distribution, Lai et al. (1999) and Habib et al. (2001a) showed through simulation experiments that the Pearson's sample correlation results in overestimation that depends on the magnitude of data skewness. This is relevant to us because rainfall data at small time scales exhibit lack of normality for the following two reasons: 1) the frequency distributions are significantly skewed for a given rainy event, and 2) rainfall exhibits intermittency. Transforming the data into having normality and applying mixed distribution models has been proposed as a solution to this problem (Shimizu 1993; Habib et al. 2001a). Following these studies, we partitioned rainfall into four classes: zero rain at both stations [0, 0], zero rain at one station and positive rain at the other [$R(x_1, y_1)$*, 0] and [0, $R(x_2, y_2)$*], and positive rain at both stations [$R(x_1, y_1)$, $R(x_2, y_2)$]. For a sample size of $N$, the four cases have sample sizes of $n_0$, $n_1$, $n_2$, and $n_3$, where $n_0 + n_1 + n_2 + n_3 = N$. For each of the last three classes, we assessed whether the data or their transforms are normally distributed. We considered two commonly used parametric transformations: square root and lognormal. We used the root-mean-square error (rmse) to measure the discrepancy between the cumulative distribution function of the data (or of their transforms) and the expected normal cumulative distribution function. For a pair of gauges or radar pixels, we partitioned the rainfall measurements into the four classes mentioned above, and calculated the resulting rmse in each of the three classes (excluding the class with both zero rain measurements). Repeating this calculation for every pair of gauges or radar pixels results in a number of rmse values in each class. We calculated the mean and distribution of the rmse values in each class, and presented it in Table 1 for TEFLUN-B. For all cases, we found, like Shimizu (1993) and Habib et al. (2001a), that the logarithmically transformed data are relatively close to normality. We reached the same conclusion for TRMM-LBA (rmse values not given here). We remark that other parametric distributions such as gamma (Kedem et al. 1990) or

TABLE 1. Distribution of rmse resulting from the discrepancy between the cumulative distribution function of the TELFLUN-B data (or of their square root and lognormal transforms) and the expected normal cumulative distribution function.

| | | Original | | Square root | | Lognormal | |
|---|---|---|---|---|---|---|---|
| | | Mean | Std dev | Mean | Std dev | Mean | Std dev |
| 15 min (gauge) | $R(x_1, y_1)$* | 0.6443 | 0.1351 | 0.4724 | 0.1087 | 0.2960 | 0.0732 |
| | $R(x_2, y_2)$* | 0.6403 | 0.1429 | 0.4565 | 0.1112 | 0.2706 | 0.0755 |
| | $R(x_1, y_1)$ | 0.6484 | 0.0673 | 0.4171 | 0.0483 | 0.1753 | 0.0210 |
| | $R(x_2, y_2)$ | 0.6678 | 0.0802 | 0.4354 | 0.0538 | 0.1793 | 0.0230 |
| Radar | $R(x_1, y_1)$* | 0.8690 | 0.0772 | 0.6348 | 0.0563 | 0.3627 | 0.0329 |
| | $R(x_2, y_2)$* | 0.8611 | 0.0710 | 0.6198 | 0.0494 | 0.3450 | 0.0293 |
| | $R(x_1, y_1)$ | 0.8096 | 0.0525 | 0.5154 | 0.0299 | 0.1700 | 0.0152 |
| | $R(x_2, y_2)$ | 0.8038 | 0.0485 | 0.4901 | 0.0375 | 0.1589 | 0.0139 |

nonparametric distributions obtained through the use of transformations, such as one based on Hermite polynomials (Journel and Huijbregts 1978), may result in better estimation properties of the sought correlation. However, investigations are needed to determine the robustness of these estimators with respect to sample size.

Our rainfall distribution model can be described as bivariate mixed lognormal (BMLN). This model can be fully characterized by 12 parameters: $\delta_0$, $\delta_1$, $\delta_2$, $\mu_1^*$, $\mu_2^*$, $\mu_1$, $\mu_2$, $\sigma_1^{*2}$, $\sigma_2^*$, $\sigma_1^2$, $\sigma_2^2$, and $\rho_N$. Parameters $\delta_i$ ($i = 0, 1, 2, 3$) are the probabilities of rainfall occurrence for each case. Parameters $\mu_i^*$ and $\sigma_i^*$ ($i = 1, 2$) are conditional means and standard deviations for cases $n_1$ and $n_2$. Parameters $\mu_i$ and $\sigma_i$ ($i = 1, 2$) and $\rho_N$ are, respectively, the conditional mean, standard deviation, and correlation coefficient for case $n_3$. These parameters correspond to the logarithmic transformation of the variables $R(x_1, y_1)$ and $R(x_2, y_2)$. Following Shimizu (1993), the moments of the BMLN distribution can be written as

$$E[R(x_1, y_1)] = \delta_1 \exp[\mu_1^* + (\sigma_1^{*2}/2)] + \delta_3 \exp[\mu_1 + (\sigma_1^2/2)], \quad (3a)$$

$$E[R(x_2, y_2)] = \delta_2 \exp[\mu_2^* + (\sigma_2^*/2)] + \delta_3 \exp[\mu_2 + (\sigma_2^2/2)], \quad (3b)$$

$$E[R(x_1, y_1)R(x_2, y_2)] = \delta_3 \exp\left[\mu_1 + \mu_2 + \frac{(\sigma_1^2 + \sigma_2^2 + 2\sigma_1\sigma_2\rho_N)}{2}\right], \quad (3c)$$

$$\mathrm{Var}[R(x_1, y_1)] = \delta_1 \exp(2\mu_1^* + 2\sigma_1^{*2}) + \delta_3 \exp(2\mu_1 + 2\sigma_1^2) - E[R(x_1, y_1)]^2, \quad \text{and} \quad (3d)$$

$$\mathrm{Var}[R(x_2, y_2)] = \delta_2 \exp(2\mu_2^* + 2\sigma_2^{*2}) + \delta_3 \exp(2\mu_2 + 2\sigma_2^2) - E[R(x_2, y_2)]^2. \quad (3e)$$

An expression for correlation can be found by inserting these expressions into (1), and the sample correlation can be calculated by using the sample estimates of these expressions.

To summarize, our approach of estimating correlation involves the following steps: 1) partitioning rainfall into four classes; 2) transforming the data in each class (excluding the class containing zero rain at both stations) into normality using lognormal transformation; 3) estimating the parameters of the BMLN model using the transformed data; and, finally, 4) estimating correlation by inserting the sample estimates of the parameters into (1). Besides better correlation estimates, the construction of such a model allows the calculation of estimation errors through Monte Carlo simulation.

### *b. Correlation function model fitting*

The literature contains a variety of approximating functions that reasonably describe the spatial correlation function over separation distance. Usually the small-scale rainfall variability is modeled with the exponential correlation functions (e.g., Stol 1972). Alternatively, it can be approximated with the Bessel function. However, Rodriguez-Iturbe and Mejia (1974) showed that there is no significant difference when either function is fitted to the correlations. It was pointed out by Baachi and Kottegoda (1995) that the available data are not usually sufficient for statistical discrimination between different kinds of functions. We chose the following three-parameter exponential model, which is quite flexible:

$$r(h) = \theta_0 \exp[-(h/\theta_1)^{\theta_2}], \qquad (\theta_0 \geq 0,\ \theta_1 > 0,\ \theta_2 \geq 0), \quad (4)$$

where $\theta_0$ is a measure of local decorrelation, that is, the correlation value at $h = 0$, $\theta_1$ is the correlation distance, and $\theta_2$ is the shape factor. The difference $1 - \theta_0$ is known as the ''nugget effect.'' A nonzero nugget could arise from one or a combination of the following phenomena: random measurement error, absence of adequate stations sufficiently close to one another to correctly determine the shape of the correlation function at very small separation distances, and microscale natural variability of rainfall (Journel and Huijbregts 1978; De Marsily 1986). We obtained the ''best''-fit parameters

in the least squares sense; that is, the sum of the weighted squared difference between the model and data is minimized. The weights were assigned inversely proportional to the standard error of the estimates determined by Monte Carlo simulation using the model described in the previous section. We used the Levenberg–Marquardt optimization technique (Press et al. 1988), which is a particular strategy for iteratively searching for the best fit.

### c. Point-to-area conversion

Another concern with the use of the correlation function is the mismatch in scales between the gauge- and radar-derived values. Because the variability of rainfall fields strongly depends on the scale at which the fields are considered, appropriate methods need to be developed to bring these two statistics to the same spatial scale.

Consider the random field $R_A(x, y)$ obtained by averaging the rainfall point process $R(x, y)$ over a square of sides $L$. These spatial averages usually have a narrower probability distribution function than those associated with point data (Vanmarcke 1983) and, consequently, a smaller variance. The variance of these spatial averages can be related to the point variance using the variance function $\gamma(L, L)$ as discussed by Vanmarcke (1983) through

$$\mathrm{Var}[R_A(x, y)] = \mathrm{Var}[R(x, y)]\gamma(L, L), \qquad \text{where} \tag{5a}$$

$$\gamma(L, L) = \left(\frac{2}{L}\right)^2 \int_0^L dh_x \int_0^L dh_y \left(1 - \frac{h_x}{L}\right) \times \left(1 - \frac{h_y}{L}\right)\rho(h), \tag{5b}$$

where $h_x$ and $h_y$ are the separation distances in $x$ and $y$ direction, respectively, and $h = (h_x^2 + h_y^2)^{1/2}$. Vanmarcke (1983) derives the following expression for the covariance of $R_A(x, y)$:

$$\mathrm{Cov}_A[h] = \frac{\mathrm{Var}[R(x, y)]}{4L^4}[\Delta(L + h_x, L + h_y) + \Delta(L - h_x, L + h_y) + \Delta(L + h_x, L - h_y) + \Delta(L - h_x, L - h_y) - 2\Delta(h_x, L + h_y) - 2\Delta(h_x, L - h_y) - 2\Delta(L - h_x, h_y) - 2\Delta(L - h_x, h_y) + 4\Delta(h_x, h_y)], \tag{6}$$

where $\Delta(L, L') = (LL')^2\gamma(L, L')$.

The correlation function of $R_A(x, y)$ can be calculated from

$$\rho_A(h) = \mathrm{Cov}_A[h]/\mathrm{Var}[R_A(x, y)]. \tag{7}$$

### d. Covariance

The covariance $\mathrm{Cov}[h]$ of the rainfall point process $R(x, y)$ can be defined as

$$\begin{aligned}\mathrm{Cov}[h] &= E[R(x_1, y_1)R(x_2, y_2)] \\ &\quad - E[R(x_1, y_1)]E[R(x_2, y_2)] \\ &= \{\mathrm{Var}[R(x_1, y_1)]\ \mathrm{Var}[R(x_2, y_2)]\}^{1/2}\rho(h).\end{aligned} \tag{8}$$

At zero lag the covariance becomes the variance. Equation (8) requires (spatial) stationarity of the rainfall field with respect to the moments of the first two orders, and the isotropy of the covariance. Similarly, the covariance function $\mathrm{Cov}_A[h]$ for the random field $R_A(x, y)$ can be expressed as

$$\mathrm{Cov}_A[h] = \{\mathrm{Var}[R_A(x_1, y_1)]\ \mathrm{Var}[R_A(x_2, y_2)]\}^{1/2}\rho_A(h). \tag{9}$$

### e. Variogram

Cressie (1993, section 2.4) argues that a variogram is preferred to correlation, because the estimate of the latter (using Pearson's formula) is heavily affected by bias and trend contamination errors. The variogram is defined as the variance of the difference between the two values assumed by $R(x, y)$ at two locations,

$$2\Gamma(h) = \mathrm{Var}[R(x_1, y_1) - R(x_2, y_2)], \tag{10}$$

where $2\Gamma(h)$ is the variogram of the process. Equation (10) assumes that $R(x, y)$ is intrinsically stationary, which means stationarity in the mean and isotropy in $\Gamma(h)$. This assumption is weaker than (8), because here no assumption about the population variance is required. This is an important advantage of the variogram because the estimation of variance is sensitive to the sample size used. This is why variogram is often used rather than covariance.

The classical method-of-moments estimator of the variogram is (Matheron 1963)

$$2\hat{\Gamma}(h) = \frac{1}{n(h)}\sum_{i,j}^{n(h)} [R(x_i, y_i) - R(x_j, y_j)]^2, \tag{11}$$

where $n(h)$ is the number of data pairs separated by lag $h$. As pointed out by Omre (1984) and Cressie (1993), a concern with (11) is that it shows little robustness with

respect to nonnormality of the difference $R(x_i, y_i) - R(x_j, y_j)$, although this difference (for rainfall) is generally less skewed than the individual random variables $R(x_i, y_i)$ and $R(x_j, y_j)$, which are directly involved in the calculation of correlation. As an alternative, we may estimate the variogram by expanding (10) and calculating the sample estimates of the resulting expressions from the BMLN model. However, this comes at the cost of calculating the mean, variance, and correlation coefficient, which are all subject to estimation error. In this study, we used the classical estimator (11).

### *f. Scaling characteristics*

A number of studies have shown that the rainfall field obeys scaling laws. These studies were carried out using rain gauge network data (e.g., Olsson and Niemczynowicz 1996; Jothityangkoon et al. 2000), ground-based radar data (e.g., Gupta and Waymire 1990, 1993; Over and Gupta 1994, 1996), and satellite data (e.g., Lovejoy and Schertzer 1995). Scaling implies that small- and large-scale statistical properties are related to each other by operations involving only the scale ratio. Unlike correlation and the variogram, which give only the second-order moment statistics, scaling has the ability to provide the full distribution function across a large range of spatial scales. Although it is quite useful to compare the spatial scaling properties of gauge- and radar-rainfall fields using a large range of moment orders, the gauge networks used in this study covered areas that are not large enough to perform such analyses. However, it is possible to study the scaling of the second-order moments such as correlation with respect to the separation distance, that is,

$$\rho(h) = mh^{-k}. \tag{12}$$

The Hurst exponent, an important statistics used to characterize variability, is analytically related to the exponent $k$. In (12), $m$ and $k$ are constants. We estimated the scaling exponent $k$ as a slope of the regression equation ''$\log[h]$ versus $\log[\rho(h)]$'' obtained by logarithmically transforming (12),

$$\log[\rho(h)] = \log[m] - k \log[h]. \tag{13}$$

We applied the Durbin–Watson test to decide whether the relation (13) is applicable. This test assesses the randomness in the residuals (Neter and Wasserman 1974); absence of randomness indicates failure of the scaling relationship. We used the significance level of 0.05 in the statistical testing.

## 4. Implementation

### *a. Time scale*

In order to compare the spatial statistics obtained from gauge- and radar-rainfall fields, we had to first decide on the appropriate time scale for comparison. As is known, a radar snapshot represents a volume average of the rain rate. Such a measurement has to be compared with accumulation over some time at the surface, because it takes raindrops several minutes to fall from the top of the column to the surface. However, the optimum number of minutes to be used in the time accumulation is open to question. After comparing radar rainfall to gauge rainfall accumulated across a range from 1 min to 1 h, Habib and Krajewski (2002) found better agreement between the radar snapshot estimates and the gauge observations if the latter were accumulated over time intervals ranging from 5 to 15 min. The GVP team used an accumulation time of 7 min in the derivation of 2A53 (Marks et al. 2000). Based on these results, we chose 5- (which is commensurate with the WSR-88D sampling frequency) and 15-min gauge accumulation times for comparison with the radar products. These two time scales could be considered as the lower and upper bounds for the optimum accumulation time required to compare radar snapshots with gauge rainfall.

### *b. Estimating correlation model and its uncertainty*

In a random function theory, the correlation estimate is a random variable with a probability distribution function (PDF) implicitly defined by the sample size and the joint distribution of the variables for which the estimate is needed. The mean of this PDF is often considered as the ''best estimate'' of correlation. The standard deviation of this PDF can be used as a measure of the expected magnitude of estimation error. To obtain the correlation estimate and its uncertainty, we used the following procedure: 1) for every pair of points (gauges or radar pixels), estimate the parameters $\delta_0$, $\delta_1$, $\delta_2$, $\mu_1^*$, $\mu_2^*$, $\mu_1$, $\mu_2$, $\sigma_1^*$, $\sigma_2^*$, $\sigma_1$, $\sigma_2$, and $\rho_N$, and get the sample size; 2) generate a single realization of the moments of rainfall from the BMLN model with the same sample size and parameter estimates, and then calculate the correlation estimate; 3) repeat step 2 1000 times; and 4) from the ensemble of the 1000 correlation estimates, calculate the mean and standard deviation. The mean and the standard deviation are the correlation estimate and its uncertainty, respectively. In step 3 above we set the total number of realizations as 1000, following Habib et al. (2001a), who reported that on the order of 1000 data points are required to estimate correlation to within $\pm 0.02$ at the 95% confidence level. Monte Carlo results presented in this study use this value except where otherwise stated.

Once we obtained the correlation estimate and its uncertainty for every separation distance between gauges or radar pixels, the next step was to search for the correlation model fit. The correlation model fit is subject to sampling uncertainty as a result of the uncertainty in the correlation estimates themselves. We obtained the best-fit correlation model in the manner explained in section 3b. To obtain the associated correlation model uncertainty, we followed these steps. 1) For every

BMLN model parameter (except $\rho_N$), we developed an approximating function that describes the variation of the parameter values with separation distance. 2) We selected several separation distances ranging from 0 to 8 km. 3) For each separation distance selected, we calculated the correlation from the best-fitted correlation model, obtained the BMLN model parameters (except $\rho_N$) from the approximating functions developed, and got the sample size from the data. 4) We calculated $\rho_N$ using the correlation and other model parameters obtained in step 3. We chose to solve for $\rho_N$ analytically using the remaining BMLN model parameters and the correlation obtained from the fitted model so that the correlation obtained by simulating from the BMLN model matches, on average, the correlation obtained from the fitted model. 5) For each separation distance selected, we generated a single realization of the moments of rainfall using all the BMLN model parameters and the sample size, and then calculated the corresponding correlation estimate. 6) We repeated step 5 1000 times, and obtained the two-standard-deviation of the correlation estimates from this ensemble. 7) Last, we obtained the correlation model uncertainty by fitting three-parameter exponential functions to the scatter of the two-standard-deviation with distance.

In step 1 above, modeling the BMLN parameters as a function of distance implies that $\delta_1 = \delta_2$, $\mu_1 = \mu_2$, $\sigma_1 = \sigma_2$, $\mu_1^* = \mu_2^*$, and $\sigma_1^* = \sigma_2^*$. We show in section 5 that the parameters $\delta_3$, $\mu_1$, and $\sigma_1$ are weakly sensitive (or insensitive) to $h$, while the parameters $\delta_1$, $\mu_1^*$, and $\sigma_1^*$ are strongly sensitive to $h$. After examining several types of functions, we came to the conclusion that the BMLN model parameters could be modeled with the following four-parameter exponential model:

$$S = c_0 + c_1[1 - \exp(-h/c_2)^{c_3}],$$
$$(c_0 \geq 0,\ c_1 \geq 0,\ c_2 > 0,\ c_3 \geq 0), \quad (14)$$

where $S$ is $\delta_1$, $\mu_1^*$, or $\sigma_1^*$, and the $c_i$s are fit parameters.

## 5. Results and discussion

### *a. Spatial correlation function*

In Fig. 2 we present the estimated spatial correlations between pairs of gauges as a function of the distance between them, as well as the analytic fit to the correlations, at 5- and 15-min rain accumulation times. Table 2 presents the fit parameters and the performance of the fit in terms of rmse. As can be seen from Table 2, the correlation distance is on the order of 4–5 km for both locations. As expected, the correlation distance increases with temporal aggregation of the process. The nugget parameter is under 5%, which is commensurate with the tipping-bucket rain gauge measurement error as estimated by Habib et al. (2001b) and Ciach (2003). The shape parameters are slightly higher than one in all cases. This implies that the correlation values obtained using our three-parameter exponential models for distances shorter (longer) than the correlation distances are slightly higher (lower) than those obtained using the commonly used two-parameter exponential models.

It can be seen from Fig. 2 that uncertainty in the correlation estimates is quite large. Apparently 2-months-long field campaigns are not long enough to estimate correlation to within a high accuracy. To estimate confidence limits on the fitted correlation model, we first modeled the BMLN parameters as a function of distance. As shown in Fig. 3 the parameters associated with the measurement of positive rain at both stations are almost insensitive to the separation distance, while those parameters associated with the measurement of positive rain only at one of the two stations show strong dependence on the separation distance. For the latter statistics, we settled on four-parameter exponential fit models of the form (14) after examining several models. The parameter estimates (except for probabilities of rain, which are higher for TRMM-LBA) are mostly similar for both locations. However, a worrisome scatter in the parameter estimates at zero lag is observed for TRMM-LBA. This may indicate that the quality of the TRMM-LBA gauges may not be very high.

The uncertainty bounds of the gauge-derived correlation model are overplotted in Fig. 2. The bounds explain most of the scatter observed in TEFLUN-B correlation estimates. For TRMM-LBA, a considerable number of sample correlations fall outside the region bounded by the model uncertainty, however, the uncertainty bounds still cross most of the sample correlation uncertainty bars. The uncertainty bounds generally show large uncertainty in the correlation model.

To obtain the radar data–based correlation function, we used horizontal, vertical, and diagonal transects to get the pixel separation distances. This results in separation distances of 2.00, 2.83, 4.00, 4.47, 5.66, 6.00, 6.32, 7.21, 8.00, 8.25, and 8.94 km. In Fig. 4 we present radar-derived correlation estimates as a function of the pixel separation distance, as well as the analytic fit to the correlations. The uncertainty in the radar-derived correlation estimates is very small, unlike the gauge-derived values. The nugget parameter for TEFLUN-B is 8% with an rmse of 0.006, while it is zero for TRMM-LBA with an rmse of 0.017. One would normally expect the nugget for radar-based correlation to be nonzero, because part of the nugget comes from the random measurement, which is significant in radar-rainfall fields. Thus, the zero nugget obtained for TRMM-LBA indicates the inability of the 2-km radar pixel to resolve the nugget accurately.

In Fig. 5 we compared the point and area correlation functions estimated from rain gauges. The area correlations are higher than the point correlations at all separation distances. This is expected because of the fact that spatial variability decreases for averaged process. We note that the magnitude of the point–area correlation discrepancy varies as a function of distance, with larger discrepancies observed at smaller distances.

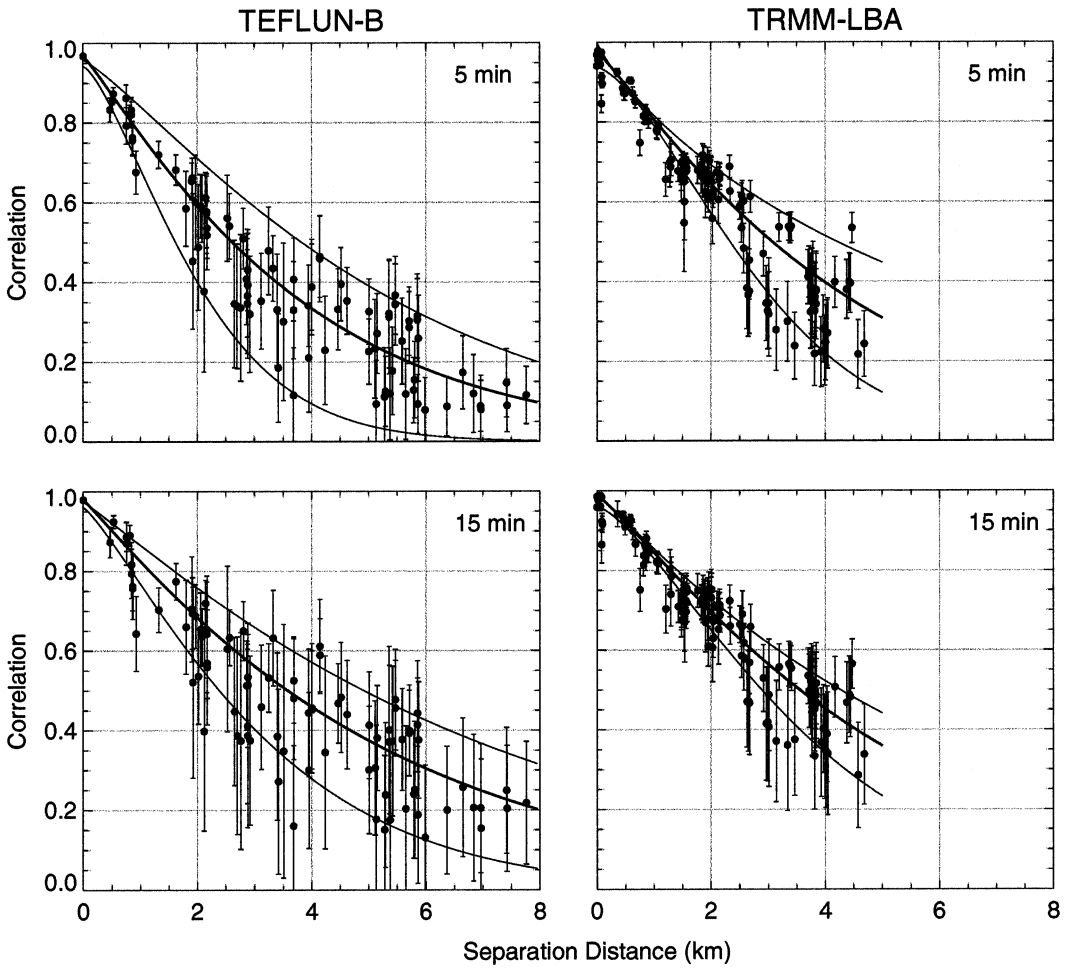


FIG. 2. Correlations and spatial correlation functions estimated from the rain gauge cluster at temporal resolutions of (top) 5 and (bottom) 15 min, for (left) TEFLUN-B and (right) TRMM-LBA. The light lines indicate the 2-std-dev sampling uncertainty bounds.

Superimposed in Fig. 5 is the area correlation function derived from radar-rainfall fields. The correlation structure obtained from radar falls faster than those obtained from gauges. For distances shorter than about 5 km, the radar-derived correlation is always lower than the gauge-derived correlation. A summary of the fitted parameters is given in Table 3. The largest discrepancy between the gauge- and radar-derived correlation function lies in the shape parameter: the radar-derived shape parameter is 0.5–0.6 times that of the gauge-derived parameter.

TABLE 2. Summary of spatial correlation function parameters estimated from the rain gauge clusters. The local decorrelation, correlation distance, and shape parameters are obtained from the fitted Eq. (4).

| Expt | Temporal resolution (min) | $\theta_0$ | $\theta_1$, km | $\theta_2$ | Rmse |
|---|---|---|---|---|---|
| TEFLUN-B | 5 | 0.96 | 3.79 | 1.11 | 0.086 |
| | 15 | 0.97 | 5.18 | 1.06 | 0.109 |
| TRMM-LBA | 5 | 0.97 | 4.37 | 1.11 | 0.077 |
| | 15 | 0.98 | 4.93 | 1.15 | 0.061 |

Next, we discuss the probable sources of uncertainty that may have caused the discrepancy between gauge- and radar-derived correlation functions. There are four potential sources of uncertainty that may have caused this discrepancy. These are 1) uncertainty resulting from random error in gauge rainfall, 2) uncertainty resulting from a small sample size used to calculate gauge-derived correlation, 3) uncertainty resulting from a less-than-optimum location of the sampling points in the radar image or an insufficient number of sampling points, and 4) uncertainty resulting from random errors in radar rainfall. We believe that the random error in gauge rainfall is greatly minimized by the density and high quality of gauges, and sufficient temporal aggregation to average out the random errors. This is also supported by the small nugget values (under 5%) obtained for gauge-rainfall fields. We, therefore, concentrated on the last three sources of uncertainty.

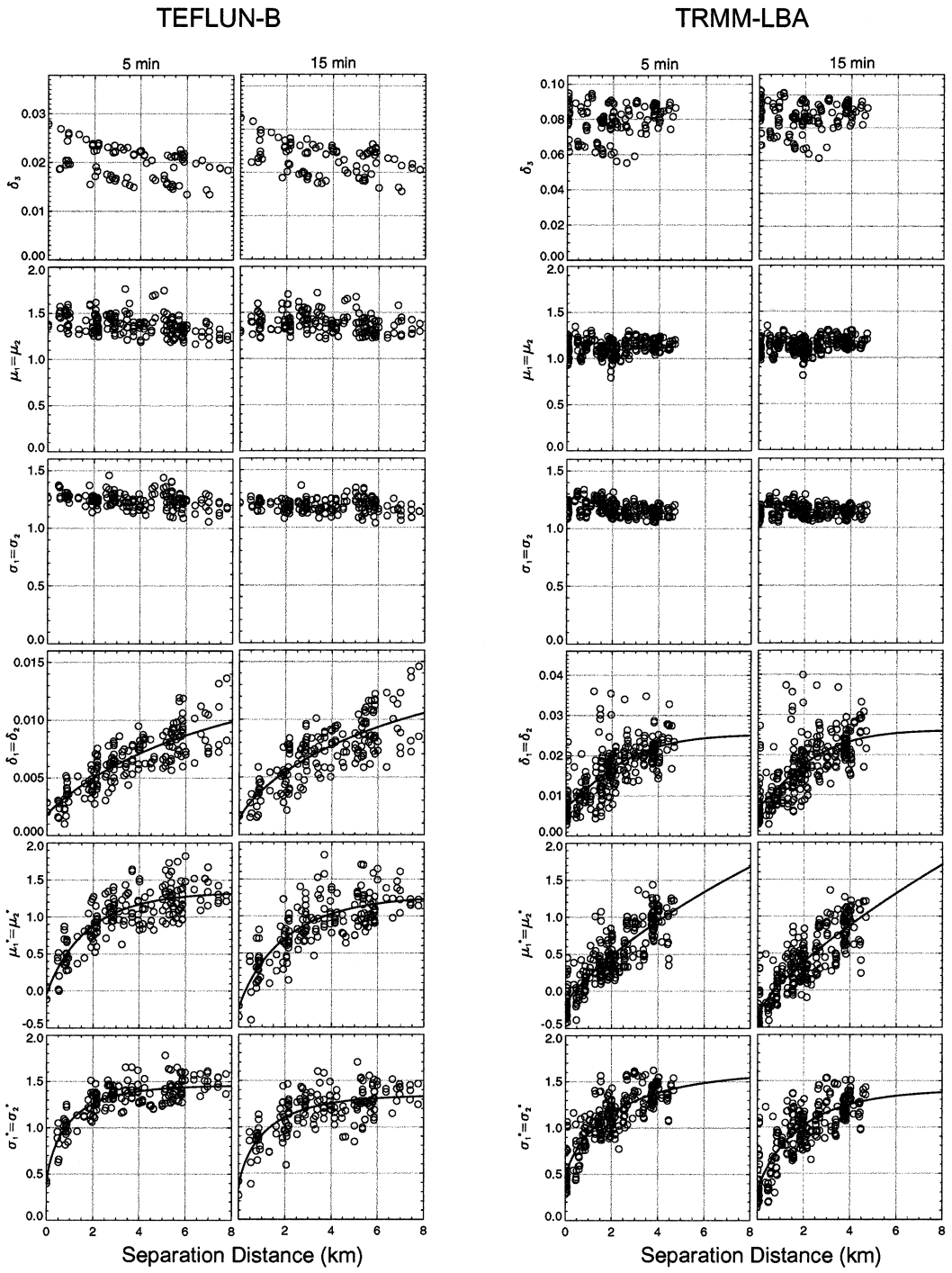


FIG. 3. The BMLN model parameters as a function of gauge separation distance.

Earlier, in Fig. 2, we showed the sampling uncertainty bounds for the gauge-derived correlation model. To examine how much this sampling uncertainty could explain the discrepancy between gauge- and radar-derived correlation functions, we integrated the uncertainty bounds of the gauge point correlation function over 2 km $\times$ 2 km, and compared them to the radar-derived correlation function in Fig. 5. The sampling uncertainty could only explain the discrepancy at separation distances exceeding about 2 (3.5) km at 5 (15) min accumulation.

The third source of uncertainty arises because of the fact that the smallest separation distance at which we could compute correlation from radar is 2 km. From

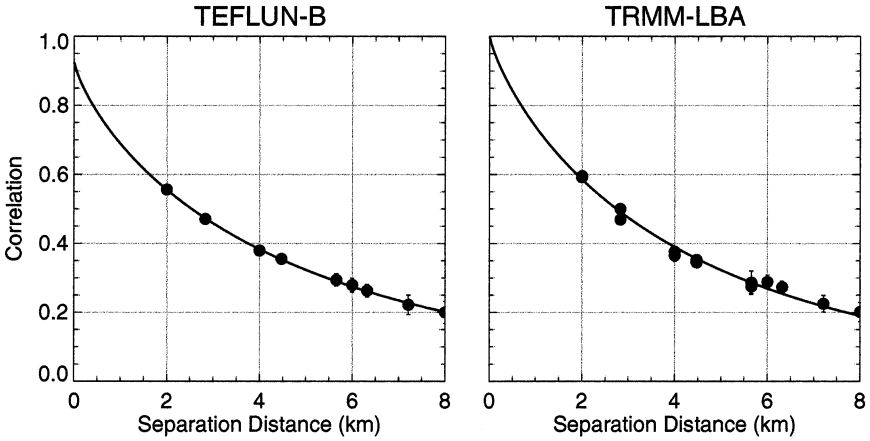


FIG. 4. Correlations and spatial correlation functions estimated from radar-rainfall fields.

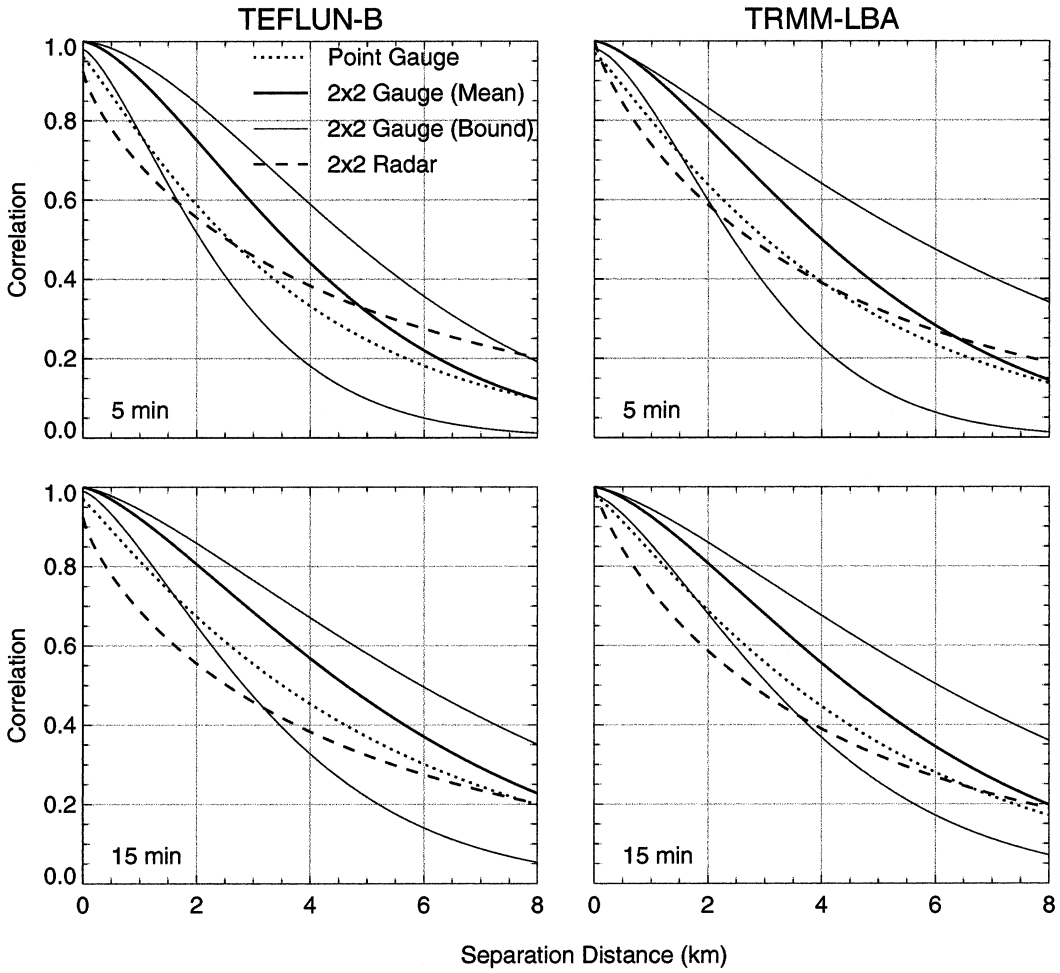


FIG. 5. Spatial point and area correlation functions estimated from gauge-rainfall fields, and the uncertainty bound for the area correlation function. Also shown is the correlation function estimated from radar-rainfall fields.

TABLE 3. Comparison of the fitted spatial correlation function parameters estimated by (i) integrating the correlation function of gauge point intensities over 2 km × 2 km, and (ii) calculating directly from radar rain field.

| Expt | Sensor | Temporal resolution (min) | $\theta_0$ | $\theta_1$, km | $\theta_2$ |
|---|---|---|---|---|---|
| TEFLUN-B | Gauge | 5 | 1.00 | 4.56 | 1.51 |
| | | 15 | 1.00 | 6.03 | 1.39 |
| | Radar | Snapshot | 0.92 | 4.70 | 0.79 |
| TRMM-LBA | Gauge | 5 | 1.00 | 5.12 | 1.48 |
| | | 15 | 1.00 | 5.75 | 1.46 |
| | Radar | Snapshot | 1.00 | 4.30 | 0.82 |

TABLE 4. Relative error of rainfall rate derived from a reflectivity-based power-law relationship as a function of the uncertainty of reflectivity measurement. Notice that in the fourth column, the first error figure in each interval is higher than the second figure because higher error corresponds to smaller *Z*.

| Expt | *Z* (dBZ) | Std dev of $\Delta Z$ (dBZ) | $\Delta R/R$ (%) |
|---|---|---|---|
| TEFLUN-B | 10–15 | 4.9 | 36–23 |
| | 15–20 | 5.2 | 25–19 |
| | 20–30 | 6.1 | 22–15 |
| | 30–50 | 8.6 | 21–12 |
| TRMM-LBA | 10–15 | 5.3 | 39–25 |
| | 15–20 | 4.5 | 22–16 |
| | 20–30 | 5.2 | 19–12 |
| | 30–50 | 7.3 | 17–10 |

classical sampling theory in time series analysis, the Nyquist frequency, $f_N = 2/(2\Delta)$, is the highest frequency that can be detected with data sampled at intervals $\Delta$. The correlation distance (e.g., 4.70 km for TEFLUN-B and 4.30 km for LBA radar-rainfall fields) is close to $2\Delta = 4.0$ km, so the shape of the correlation structure at small separation distances is difficult to estimate. This, in turn, makes difficult the estimation of the nugget and shape parameters of the correlation function model in particular.

The last source of uncertainty arises because of the presence of significant random errors in radar-rainfall fields. Using the vertical profile of reflectivity measurements obtained from the 915-MHz profilers deployed during both TRMM experiments, we compared in Fig. 6 the reflectivity measured at the lowest reliable profiler gate height (a few hundred meters) $Z_0$ with the reflectivity measured at the gate height close to 1.5 km (height of the rain map) $Z_{1.5}$. We point out that the elevation of 1.5 km is well below the freezing level, and so brightband effects are avoided. Figure 6 shows a significant random variation between $Z_0$ and $Z_{1.5}$; let $\Delta Z = Z_{1.5} - Z_0$. Table 4 shows the standard deviation of $\Delta Z$, conditional on $Z_0$. Here, $Z_{1.5}$ could differ from $Z_0$ by about 4–9 dBZ. Because we are comparing radar-rainfall fields (derived from $Z_{1.5}$) with surface gauge–rainfall fields, the significant deviation of $\Delta Z$ from zero causes a discrepancy between the rainfall statistics estimated from both fields even if the $Z_{1.5}$ data were perfect. Let us examine the extent of the influence of $\Delta Z$ on the rainfall estimate *R*. From the power law $R = \omega Z^{\delta}$, the uncertainty of *R* due to $\Delta Z$ can be expressed as

$$\frac{\Delta R}{R} = \frac{(Z + \Delta Z)^{\delta} - (Z - \Delta Z)^{\delta}}{2Z^{\delta}} 100\%. \qquad (15)$$

Letting $\delta = 0.714$ (a value used in 2A53 products), the uncertainty of *R* is shown in Table 4. Assuming that the $Z_{1.5}$ data are perfect, $\Delta Z$ could cause *R* to deviate from its true value by 10%–40%. It is of course known that the $Z_{1.5}$ data are subject to additional random error sources, such as radar hardware noise and radar sampling error, which refers to the problem of inferring the mean of a radar bin given a limited number of randomly fluctuating signals. Moreover, the conversion of reflectivity to rain rate introduces other sources of random error, such as uncertainty in the *Z*–*R* relationship, natural variability of drop size distribution, hail, and so on. Hence, one can conclude the presence of significant random errors in the radar-rainfall fields.

To what extent do the random errors in radar rainfall affect the correlation estimate? We investigated this issue for different magnitudes of random errors through a data-driven Monte Carlo simulation experiment. Our

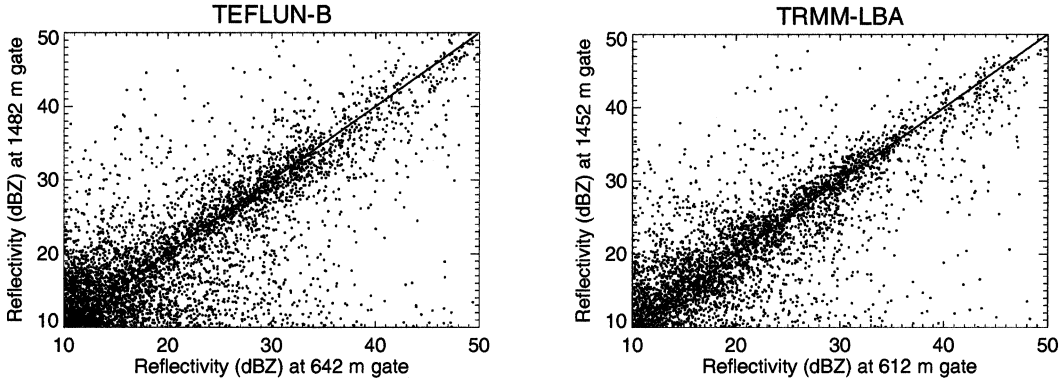


FIG. 6. Scatterplot of 50-s reflectivity measurements taken at two elevations obtained by the 915-MHz profiler.

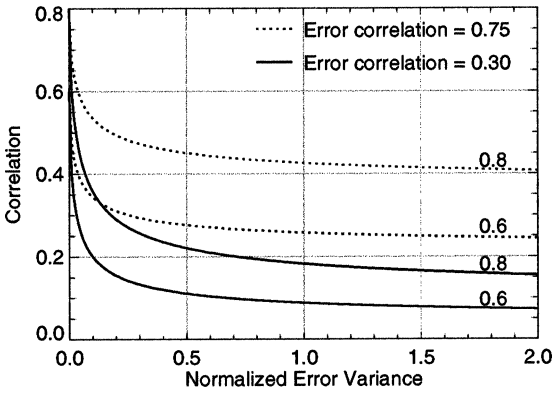


FIG. 7. Illustration of how random error affects the mean sample correlation between two random variables (with a true correlation of 0.8 and 0.6) drawn from the BMLN model. The parameters of the distributions are $\mu_1^* = 0.35$, $\mu_2^* = 0.82$, $\mu_1 = 1.36$, $\mu_2 = 1.22$, $\sigma_1^* = 0.99$, $\sigma_2^* = 1.13$, $\sigma_1 = 1.22$, $\sigma_2 = 1.28$. The rest of the parameters had the following values: $\delta_0 = 0.97$, $\delta_1 = \delta_2 = 0$, $\delta_3 = 0.03$.

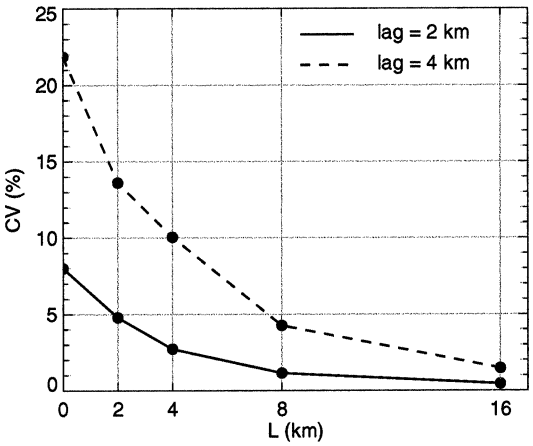


FIG. 8. Influence of averaging area on uncertainty of gauge-derived correlation estimates at a lag of 2 (solid line) and 4 (dashed line) km.

simulation had three steps: 1) generate realizations of two random variables with known true correlation coefficient; 2) contaminate the realizations with errors of a known distribution function; and 3) estimate the correlation from the error-contaminated realizations and compare it to the true correlation. We generated the rainfall realizations using the BMLN model parameters taken from two gauges and assumed the errors to have a lognormal distribution as in Smith and Krajewski (1991), Ciach and Krajewski (1999b), Anagnostou et al. (1999), and Tustison et al. (2003). We considered errors with a spatial correlation coefficient of 0.75 and 0.30. The error-contaminated realizations are obtained as a product of the realizations of the rainfall random variables and the random error. In Fig. 7 the correlation estimates obtained from the error-contaminated realizations are compared with the corresponding true correlations (0.8 and 0.6), as a function of the normalized error variance (defined as the variance of the error divided by the variance of the true rainfall random variables). The role of random errors is always to underestimate the true correlation. Notice how the correlation estimate drops significantly at very small error variances. The magnitude of the error in correlation depends on the error correlation structure; strongly correlated errors result in smaller errors, as expected. Hence, the correlation underestimated by the radar-rainfall fields could be partly explained by the random errors inherent in radar-rainfall fields at the considered space–time scale. However, we could not accurately quantify how much of the correlation underestimated by radar is attributed to random errors because of lack of information on the marginal and joint distribution functions of radar-rainfall random errors.

### *b. Space and time averages*

A common technique to reduce random error is by averaging the process in a larger space or time scale. Averaging reduces not only the random error in radar rainfall, but also the estimation uncertainty in gauge-derived correlation. In this section we examine how the correlation functions derived from radar and gauge fields compare at a variety of space–time scales. We based our analysis on TEFLUN-B radar and 15-min gauge datasets. We considered averaging areas (spatial scales) of $L \times L$, where $L = 2$, 4, 8, and 16 km. We point out that in order to consider the given spatial scales, we enlarged our region of interest depicted in Fig. 1 to an area of 32 km $\times$ 32 km.

Let us first see how the estimation uncertainty in gauge-derived correlation function decreases with increasing spatial scale, using the coefficient of variation (CV) as a measure of the estimation uncertainty. We selected two specific separation distances (2 and 4 km) and monitored how CV behaves at different spatial scales. As is evident from Fig. 8, estimation uncertainty is quite large at small spatial scales and decreases substantially as the scale of averaging increases.

In Fig. 9 we compare the gauge- and radar-derived correlation functions at various spatial scales. At small separation distances, the discrepancy between the two correlation estimates decreases with an increasing spatial scale. For example, at a separation distance of 2 km, the discrepancy in correlation is 31% at $L = 2$ km, 25% at $L = 4$ km, 14% at $L = 8$ km, and 7% at $L = 16$ km. There is a significant discrepancy between the gauge- and radar-derived correlation even at 16 km $\times$ 16 km. This suggests that the number of pixels used in the averaging may not be large enough to average out the random errors in the radar rainfall, and/or the discrepancy could be due to the other sources of problems discussed in the preceding section.

Figure 10 shows a comparison of the correlation functions estimated from hourly gauge- and radar-rainfall fields. The hourly rainfall accumulations were estimated as the sum of the four 15-min rainfall accumulations

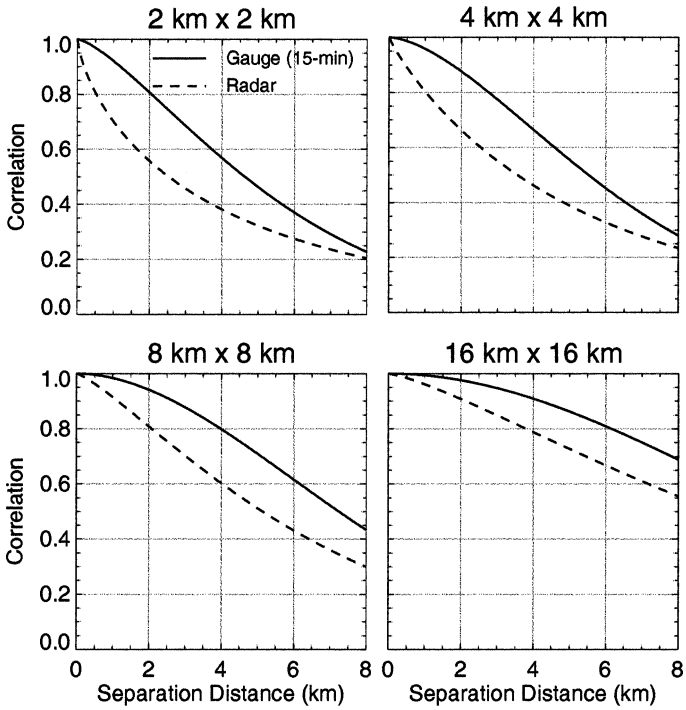


FIG. 9. Spatial correlation functions obtained from gauge- (solid line) and radar- (dashed line) rainfall fields for TEFLUN-B at various averaging areas.

within the hour. Averaging four rainfall values could not improve the discrepancy in correlation functions between radar- and gauge-derived values.

### c. Other spatial statistics

In Fig. 11 we compare the gauge- and radar-rainfall fields in terms of the covariance model. For TEFLUN-B, the discrepancy between the gauge- and radar-derived covariances is generally small, and it follows the pattern exhibited by the correlation models (except close to zero lags). For TRMM-LBA, however, the radar-derived covariances are significantly smaller than those obtained from gauges, at all lags. While the relative error in variances estimated from radar- and gauge-rainfall fields is about 0% (17%) for TEFLUN-B, it is about 67% (57%) for TRMM-LBA at 5- (15-) min rain accumulation times.

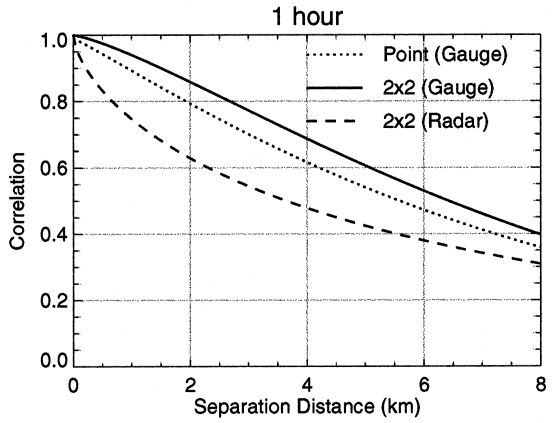


FIG. 10. Spatial correlation functions estimated from TEFLUN-B hourly gauge- and radar-rainfall fields.

Figure 12 displays the variograms estimated from gauge- and radar-rainfall fields. For TEFLUN-B, the gauge- and radar-derived variograms behave in a similar manner: the variograms initially increase until separation distances reach approximately 6 km, the approximate range of the spatial resolution, and then they remain relatively constant (at the sill value) for separation distances longer than the range. For TRMM-LBA, the gauge-derived variograms do not reach the sill level, which could be explained by the absence of sufficiently long interstation distances. The variograms of TEFLUN-B radar-rainfall fields are mostly within the scatter of those obtained from gauges, while the variograms of TRMM-LBA radar-rainfall fields are consistently lower than those obtained from gauges at all separation distances, which can be explained by the discrepancy in variance estimates.

The correlation estimates are shown on a log–log plot in Fig. 13. We tested the linearity in the log–log dependency of the correlation on separation distance, ranging from 2 to 8 km, using the Durbin–Watson test. In Table 5, $D$ is the Durbin–Watson test statistic, and $d_L$ and $d_U$ are the lower and upper bounds, respectively, such that a value of $D$ outside these bounds leads to a

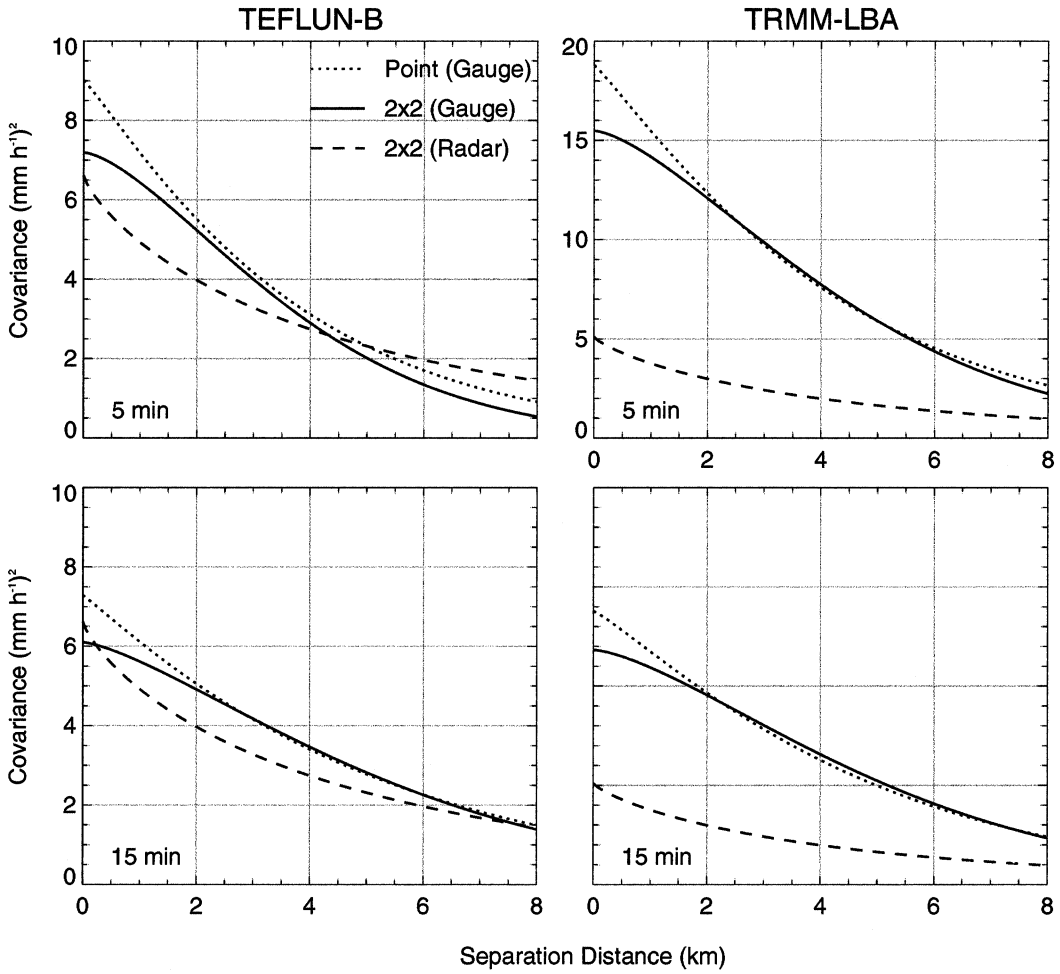


FIG. 11. Spatial covariance functions estimated from gauge- and radar-rainfall fields.

definite decision. As can be seen from Table 5, there is no definite decision regarding the linearity in TRMM-LBA rainfall fields. In principle, this means that more data are required. The TEFLUN-B radar-rainfall fields exhibit a linear pattern, while the gauge-rainfall fields do not. We remark that because the gauge-derived sample correlations are subject to large sampling uncertainty (see Fig. 2), the decisions made could well be affected by the sample size limitation.

In Fig. 14 we present the variance reduction, due to areal averaging, in terms of the area-averaged variance normalized by the variance over 2 km $\times$ 2 km. This plot is constructed using $L = 2$, 4, 8, and 16 km and connecting the calculated values with straight lines. We observe that the variance reduction generally decreases with an increasing spatial scale for both gauge and radar fields, as expected. The difference between the variance reductions obtained from gauge- and radar-rainfall fields decreases with increasing spatial scale, from 0.16 at $L = 2$ km to 0.03 at $L = 16$ km.

## 6. Application-based evaluation

We have shown the discrepancy in spatial statistics derived from gauge and radar rain fields. One of the applications in which the correlation function input is required is the quantification of gauge sampling uncertainty. In this section, we examine quantitatively to what degree the error in radar-derived correlation function affects gauge sampling uncertainty estimates.

Consider a single gauge located within a square area of size $A$. Let $\hat{R}$ be the rain rate measured with a gauge over period $t$, and say this measurement is used to estimate the rain rate $R_A$ averaged over area $A$ and period $t$.

The sampling error is

$$\varepsilon = \hat{R} - R_A. \tag{16}$$

Our interest is in the sampling uncertainty $\sigma_\varepsilon$, which is defined here as the standard deviation of $\varepsilon$. Morrissey et al. (1995) derived the following approximating equation, which requires the correlation function, to estimate $\sigma_\varepsilon$ for an arbitrary sampling network configuration:

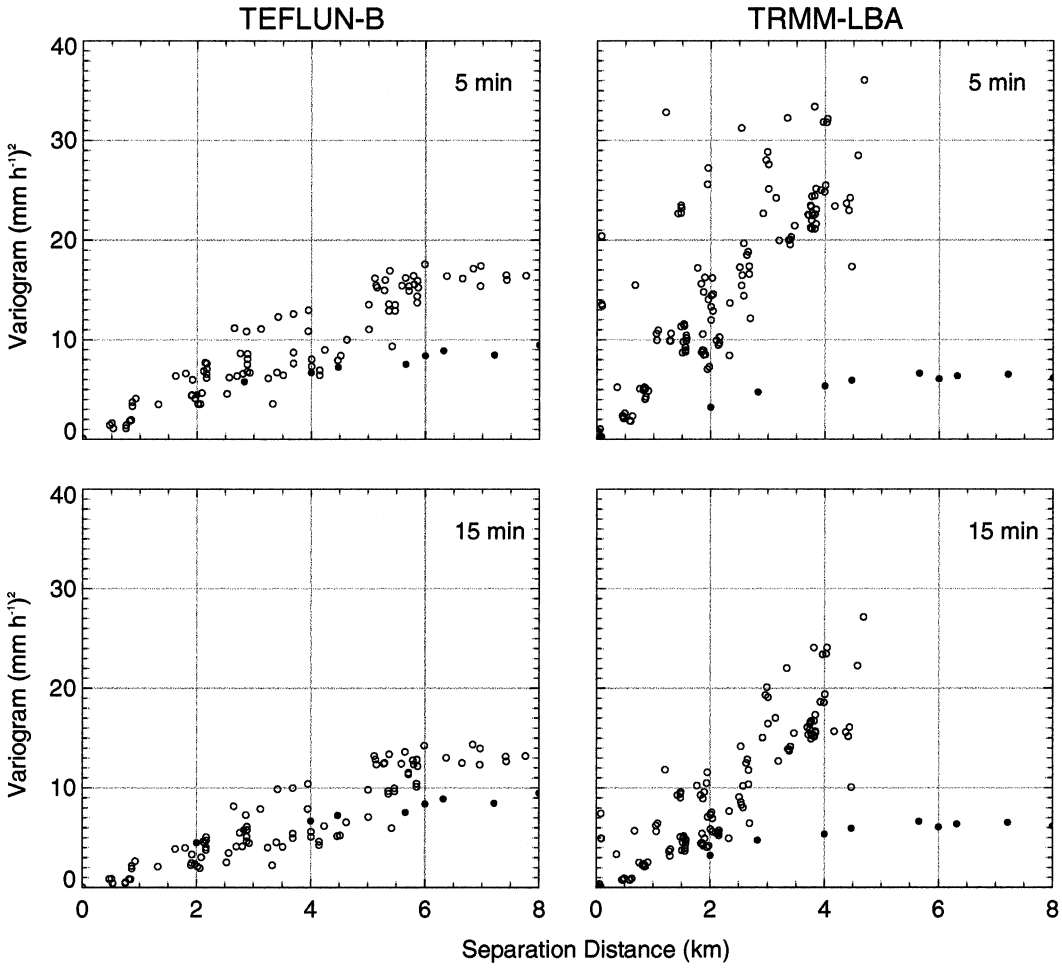


FIG. 12. Variogram estimates obtained from radar (filled circles) and gauge (open circles) rainfall.

$$\sigma_\varepsilon = \sigma_R\left[\frac{2}{n^2}\sum_{i=1}^{K-1}\sum_{j=i+1}^{K}\rho(h_{i,j})\delta(i)\delta(j) - \frac{2}{Kn}\sum_{i=1}^{K}\sum_{j=1}^{K}\rho(h_{i,j})\delta(i) + \frac{1}{K} + \frac{2}{K^2}\sum_{i=1}^{K-1}\sum_{j=i+1}^{K}\rho(h_{i,j})\right], \quad (17)$$

where $\sigma_R$ is the variance of the gauge point rainfall. The area $A$ is divided into $K$ grid boxes; the Kronecker delta function $\delta(i)$ denotes whether box $i$ contains a rain gauge. The term $\rho(h_{i,j})$ represents the rainfall spatial correlation, where $h_{i,j}$ is the distance between box $i$ and box $j$. The first term in (19) accounts for the spatial correlation among the $n$ gauges. The second term represents the average spatial correlation between each rain gauge location and all points within the averaging area. The centering of a gauge network within the averaging area decreases the magnitude of this term and results in a decrease in the sampling uncertainty. The third term represents the corrective factor of the effect that the grid system exerts on the sampling uncertainty, and for a large number of grid points this term can be neglected. The fourth term is the average spatial correlation among all $K$ points—both with and without rain gauges—within the averaging domain with respect to the average spatial correlation function.

Let us rewrite (17) as

$$\sigma_\varepsilon = \sigma_R\phi[\rho(h_{i,j}), K, n]. \quad (18)$$

For a given $K$ and $n$, the phi function $\phi[\rho, K, n]$ represents the impact on sampling uncertainty by the correlation function. Its square $\phi^2$ is sometimes called the variance reduction factor. For $n = 1$, the correlation function affects $\phi$ through the second and fourth terms in (17). Higher correlation values tend to decrease $\phi$ through the second term and increase $\phi$ through the fourth term; the dominant term depends on the spatial configuration of gauges.

Let $\hat{\phi}$ and $\phi$ denote the phi functions estimated using

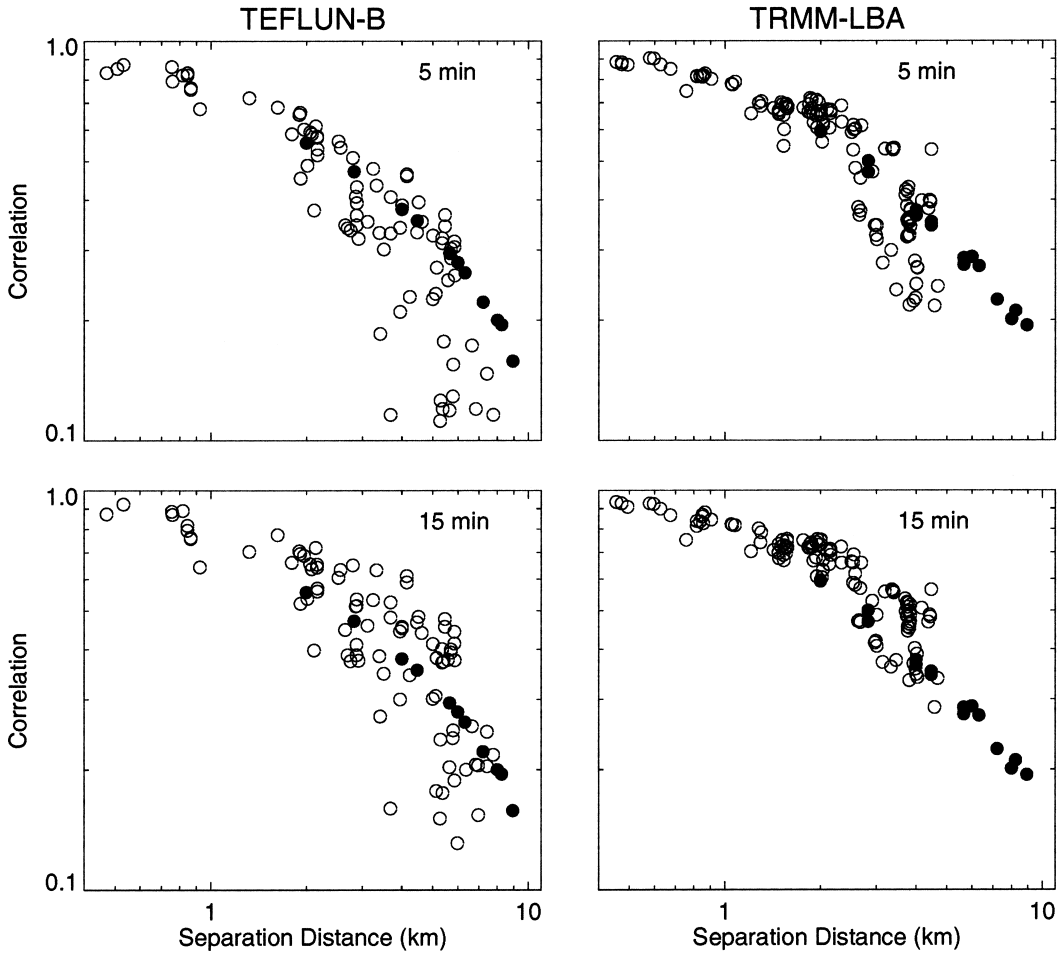


FIG. 13. Log–log plot of correlations estimated from radar (filled circles) and gauge (open circles) rainfall.

radar- and gauge-derived correlation functions, respectively. Set $A = 4$ km$^2$ (the size of radar-rainfall resolution), and $t = 15$ min. To quantify the discrepancy between $\hat{\phi}$ and $\phi$ for every gauge shown in Fig. 1, we used the relative error $\varepsilon_r$ expressed as

$$\varepsilon_r = \frac{(\hat{\phi} - \phi)}{\phi} 100\%. \quad (19)$$

The $\varepsilon_r$ values are presented in Table 6 (Table 7) for TEFLUN-B (TRMM-LBA). Overall radar-derived correlation functions overestimate the gauge sampling uncertainty by 9%–27% for TEFLUN-B and by 0%–9% for TRMM-LBA. However, there are also a few gauges in TRMM-LBA, located close to the corner of the pixels, for which the radar-derived correlation results in slight underestimation (within 4%).

## 7. Conclusions

The primary objective of the general research that led to this paper is the investigation of the ability of radar-

TABLE 5. Test of linearity pattern in log–log dependency of the correlation on distance observed in gauge- and radar-rainfall fields, based on the Durbin–Watson statistic test.

| Expt | Rainfall field | $n$ | $D$ | $d_L$ | $du$ | Conclusion on linearity |
|---|---|---|---|---|---|---|
| TEFLUN-B | 5-min gauge | 72 | 1.81 | 1.58 | 1.64 | Reject |
| | 15-min gauge | 72 | 1.85 | 1.58 | 1.64 | Reject |
| | Radar | 9 | 0.61 | 1.08 | 1.36 | Accept |
| TRMM-LBA | 5-min gauge | 67 | 1.57 | 1.57 | 1.63 | Inconclusive |
| | 15-min gauge | 67 | 1.58 | 1.57 | 1.63 | Inconclusive |
| | Radar | 14 | 1.35 | 1.08 | 1.36 | Inconclusive |

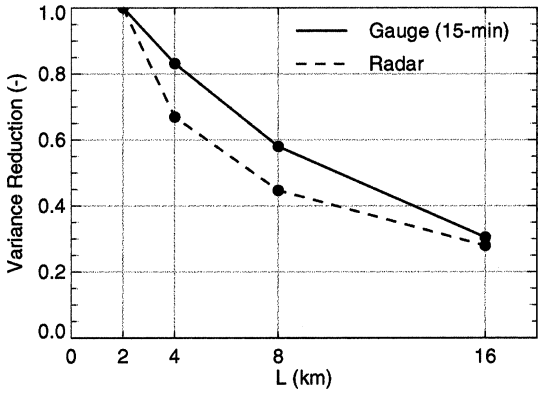


FIG. 14. Variance of area-averaged rainfall normalized by the variance of rainfall averaged over 2 km × 2 km.

TABLE 6. Comparison of $\phi$ and $\hat{\phi}$, for each TEFLUN-B gauge location shown in Fig. 1 with respect to the corresponding radar pixel.

| Label | Official No. | $\phi$ | $\hat{\phi}$ | $\varepsilon_r$ (%) |
|---|---|---|---|---|
| a | 101a | 0.34 | 0.44 | 27 |
| b | 101b | 0.34 | 0.44 | 27 |
| c | 102 | 0.48 | 0.52 | 9 |
| d | 103 | 0.46 | 0.51 | 12 |
| e | 108a | 0.35 | 0.44 | 25 |
| f | 108b | 0.36 | 0.45 | 24 |
| g | 108c | 0.40 | 0.47 | 18 |
| h | 109 | 0.36 | 0.45 | 23 |
| i | 110 | 0.34 | 0.44 | 27 |
| j | 112 | 0.34 | 0.44 | 26 |
| k | 113 | 0.36 | 0.45 | 25 |
| l | 114 | 0.44 | 0.50 | 14 |
| m | 115 | 0.45 | 0.51 | 12 |
| n | 116 | 0.42 | 0.48 | 15 |

rainfall fields to capture the small-scale spatial rainfall variability. The purpose of this paper has been to compare radar- and gauge-rainfall fields through the use of spatial statistics, such as correlation function, covariance, variogram, scaling characteristics, and variance reduction due to areal averaging. Our approach takes into account the problems associated with the traditional estimation methods, and the recognized differences in the scales of observation.

From this study it can be concluded that the radar-derived spatial statistics are subject to errors. For example, the radar-derived correlations are lower than those obtained from rain gauges at separation distances shorter than about 5 km. To quantify the effect of the errors in radar-derived spatial statistics, one must have some understanding of the context in which these statistics will be used. If the objective is to calculate the sampling uncertainty of area-averaged (4 km$^2$) rainfall estimated from one rain gauge station, the use of a radar-derived correlation function could give errors ranging from −4% to 27%.

This work should give researchers an idea about the magnitude of errors in radar-derived spatial statistics. However, 2 months of data are not large enough to draw strong conclusions. Similar studies should be performed using a larger sample size so as to provide conclusive results at different levels of space–time scales. Other effects, such as different rainfall regimes and seasonal effects, need to be addressed. The effects of other methods of spatial statistics estimation, such as those that track the rain field motion, should be analyzed. Corrective measures need to be developed to improve the accuracy of radar-derived spatial statistics.

*Acknowledgments.* This study was supported by NASA Grant NAG5-9664. We acknowledge and appreciate the assistance and cooperation of the NASA's TRMM GV personnel and are grateful to all those who collected specialized datasets in the TEFLUN-B and TRMM-LBA campaigns. We thank three anonymous reviewers for useful comments. We also thank David Marks for helpful information about the datasets.

TABLE 7. Same as in Table 6, but for TRMM-LBA.

| Label | Official No. | $\phi$ | $\hat{\phi}$ | $\varepsilon_r$ (%) | Label | Official No. | $\phi$ | $\hat{\phi}$ | $\varepsilon_r$ (%) |
|---|---|---|---|---|---|---|---|---|---|
| a | A1001 | 0.44 | 0.44 | 1 | n | A1014 | 0.39 | 0.40 | 4 |
| b | A1002 | 0.42 | 0.43 | 2 | o | N2001 | 0.55 | 0.53 | −4 |
| c | A1003 | 0.44 | 0.44 | 1 | p | N2002 | 0.54 | 0.53 | −3 |
| d | A1004 | 0.43 | 0.44 | 1 | q | N2003 | 0.45 | 0.45 | 0 |
| e | A1005 | 0.43 | 0.43 | 1 | r | N2005 | 0.55 | 0.53 | −3 |
| f | A1006 | 0.34 | 0.37 | 8 | s | N2006 | 0.36 | 0.38 | 6 |
| g | A1007 | 0.34 | 0.36 | 9 | t | N2007 | 0.37 | 0.39 | 6 |
| h | A1008 | 0.33 | 0.36 | 9 | u | N2008 | 0.37 | 0.39 | 6 |
| i | A1009 | 0.33 | 0.36 | 9 | v | N2009 | 0.37 | 0.39 | 5 |
| j | A1010 | 0.35 | 0.37 | 8 | w | N2010 | 0.43 | 0.44 | 1 |
| k | A1011 | 0.39 | 0.41 | 4 | x | N2011 | 0.44 | 0.44 | 1 |
| l | A1012 | 0.42 | 0.43 | 2 | y | N2012 | 0.44 | 0.45 | 1 |
| m | A1013 | 0.52 | 0.51 | −2 | z | N2013 | 0.44 | 0.44 | 1 |

## REFERENCES


Anagnostou, E. N., W. F. Krajewski, and J. Smith, 1999: Uncertainty quantification of mean-areal radar-rainfall estimates. *J. Atmos. Oceanic Technol.,* **16,** 206–215.

Austin, P. M., 1987: Relation between measured radar reflectivity and surface rainfall. *Mon. Wea. Rev.,* **115,** 1053–1069.

Baachi, B., and N. T. Kottegoda, 1995: Identification and calibration of spatial correlation patterns of rainfall. *J. Hydrol.,* **165,** 311–348.

Barnston, A. G., 1991: An empirical method of estimating raingage and radar rainfall measurement bias and resolution. *J. Appl. Meteor.,* **30,** 282–296.

Bell, T. L., and P. K. Kundu, 2003: Comparing satellite rainfall estimates with rain gauge data: Optimal strategies suggested by a spectral model. *J. Geophys. Res.,* **108,** 4121, doi:10.1029/2002JD002641.

Capsoni, C., F. Fedi, and A. Paraboni, 1987: A comprehensive attenuation time series generator and comparison with Olympus data meteorologically oriented methodology for the prediction of wave propagation parameters in telecommunication applications beyond 10 GHZ. *Radio Sci.,* **22,** 387–393.

Ciach, G. J., 2003: Local random errors in tipping-bucket rain gauge measurements. *J. Atmos. Oceanic Technol.,* **20,** 752–759.

——, and W. F. Krajewski, 1999a: On the estimation of radar rainfall error variance. *Adv. Water Res.,* **22,** 585–595.

——, and ——, 1999b: Radar–rain gauge comparisons under observational uncertainties. *J. Appl. Meteor.,* **38,** 1519–1525.

Cifelli, R., W. A. Petersen, L. D. Carey, and S. A. Rutledge, 2002: Radar observations of the kinematic, microphysical, and precipitation characteristics of two MCSs in TRMM-LBA. *J. Geophys. Res.,* **107,** 8077, doi:10.1029/2000JD0000264.

Cressie, N. A. C., 1993: *Statistics for Spatial Data.* Wiley and Sons, 462 pp.

Crum, T. D., R. L. Alberty, and D. W. Burgess, 1993: Recording, archiving, and using WSR-88D data. *Bull. Amer. Meteor. Soc.,* **74,** 645–653.

Datta, S., W. L. Jones, B. Roy, and A. Tokay, 2003: Spatial variability of surface rainfall as observed from TRMM field campaign data. *J. Appl. Meteor.,* **42,** 598–610.

De Marsily, G., 1986: *Quantitative Hydrogeology: Groundwater Hydrology for Engineers.* Academic Press, 440 pp.

Gebremichael, M., W. F. Krajewski, M. Morrissey, D. Langerud, G. J. Huffman, and R. Adler, 2003: Error uncertainty analysis of GPCP monthly rainfall products: A data-based simulation study. *J. Appl. Meteor.,* **42,** 1837–1848.

Germann, U., and J. Joss, 2001: Variograms of radar reflectivity to describe the spatial continuity of Alpine precipitation. *J. Appl. Meteor.,* **40,** 1042–1059.

Gupta, V. K., and E. C. Waymire, 1990: Multiscaling properties of spatial rainfall and river flow distributions. *J. Geophys. Res.,* **95,** 1999–2009.

——, and ——, 1993: A statistical analysis of mesoscale rainfall as a random cascade. *J. Appl. Meteor.,* **32,** 251–267.

Ha, E., and G. R. North, 1999: Error analysis for some ground validation designs for satellite observations of precipitation. *J. Atmos. Oceanic Technol.,* **16,** 1949–1957.

Habib, E., and W. F. Krajewski, 2002: Uncertainty analysis of the TRMM ground-validation radar-rainfall products: Application to the TEFLUN-B field campaign. *J. Appl. Meteor.,* **41,** 558–572.

——, ——, and G. J. Ciach, 2001a: Estimation of rainfall interstation correlation. *J. Hydrometeor.,* **2,** 621–629.

——, ——, and A. Kruger, 2001b: Sampling errors of tipping-bucket rain gauge measurements. *J. Hydrol. Eng.,* **6,** 159–166.

Heiss, W. H., D. L. McGrew, and D. Sirmans, 1990: Next Generation Weather Radar (WSR-88D). *Microwave J.,* **33,** 79–98.

Joss, J., and A. Waldvogel, 1990: Precipitation measurement and hydrology. *Radar in Meteorology: Battan Memorial 40th Anniversary Radar Meteorology Conference,* D. Atlas, Ed., Amer. Meteor. Soc., 577–606.

——, and R. Lee, 1995: The application of radar-gauge comparisons to operational precipitation profile corrections. *J. Appl. Meteor.,* **34,** 2612–2630.

Jothityangkoon, C., M. Sivapalan, and N. R. Viney, 2000: Tests of a space-time model of daily rainfall in southwestern Australia based on nonhomogeneous random cascades. *Water Resour. Res.,* **36,** 267–284.

Journel, A. G., and C. J. Huijbregts, 1978. *Mining Geostatistics.* Academic Press, 600 pp.

Kedem, B., L. S. Chiu, and G. R. North, 1990: Estimation of mean rain rate: Application to satellite observations. *J. Geophys. Res.,* **95** (D2), 1965–1972.

Kowalski, C. J., 1972: On the effect of non-normality on the distribution of the sample product-moment correlation function. *Appl. Stat.,* **27,** 1–12.

Krajewski, W. F., 1987: Cokriging radar-rainfall and rain gage data. *J. Geophys. Res.,* **92** (D8), 9571–9580.

——, E. N. Anagnostou, and G. J. Ciach, 1996: Effects of the radar observation process on inferred rainfall statistics. *J. Geophys. Res.,* **101** (D21), 26 493–26 502.

Kummerow, C., W. S. Olson, and L. Giglio, 1996: A simplified scheme for obtaining precipitation and vertical hydrometeor profiles from passive microwave sensors. *IEEE Trans. Geosci. Remote Sens.,* **34,** 1213–1232.

Lai, C. D., J. C. W. Rayner, and T. P. Hutchinson, 1999: Robustness of the sample correlation—The bivariate lognormal case. *J. Appl. Math. Decis. Sci.,* **3,** 7–19.

Lovejoy, S., and D. Schertzer, 1995: Multifractals and rain. *New Uncertainty Concepts in Hydrology and Water Resources,* A. W. Kundzewicz, Ed., Cambridge University Press, 111–144.

Marks, D. A., and Coauthors, 2000: Climatological processing and product development for the TRMM ground validation program. *Phys. Chem. Earth,* **25B,** 871–875.

Matheron, G., 1963: Principles of geostatistics. *Econ. Geol.,* **58,** 1246–1266.

Morrissey, M. L., J. A. Maliekal, J. S. Greene, and J. Wang, 1995: The uncertainty in simple spatial averages using raingage networks. *Water Resour. Res.,* **31,** 2011–2017.

Moszkowicz, S., 2000: Small-scale structure of rain field: Preliminary results basing on a digital gauge network and on MRL-5 Legionowo radar. *Phys. Chem. Earth,* **25B,** 933–938.

Neter, J., and W. Wasserman, 1974: *Linear Statistical Methods.* Richard D. Irwin, 667 pp.

Niemczynowicz, J., 1988: The rainfall movement: A valuable complement to short-term rainfall data. *J. Hydrol.,* **104,** 311–326.

North, G. R., and S. Nakamoto, 1989: Formalism for comparing rain estimation designs. *J. Atmos. Oceanic Technol.,* **6,** 985–992.

Olsson, J., and J. Niemczynowicz, 1996: Multifractal analysis of daily spatial rainfall distributions. *J. Hydrol.,* **187,** 29–43.

Omre, H., 1984: The variogram and its estimation. *Geostatistics for Natural Resources Characterization,* G. Verley et al., Eds., NATO ASI Series C, Vol. 1, D. Reidel, 107–125.

Over, T. M., and V. K. Gupta, 1994: Statistical analysis of mesoscale rainfall: Dependence of a random cascade generator on large-scale forcing. *J. Appl. Meteor.,* **33,** 1526–1542.

——, and ——, 1996: A space–time theory of mesoscale rainfall using random cascades. *J. Geophys. Res.,* **101** (D21), 26 319–26 332.

Pereira Fo, A. J., and K. C. Crawford, 1999: Mesoscale precipitation fields. Part I: Statistical analysis and hydrologic response. *J. Appl. Meteor.,* **38,** 82–101.

Petersen, W. A., S. W. Nesbitt, R. J. Blakeslee, R. Cifelli, P. Hein, and S. A. Rutledge, 2002: TRMM observations of intraseasonal variability in convective regimes over the Amazon. *J. Climate,* **15,** 1278–1294.

Press, W. H., B. P. Flannery, S. A. Teukolsky, and W. T. Vetterling, 1988: *Numerical Recipes: The Art of Scientific Computing.* Cambridge University Press, 818 pp.

Robinson, M., and Coauthors, 2000: Evolving improvements to

TRMM ground validation rainfall estimates. *Phys. Chem. Earth,* **25B,** 971–976.

Rodriguez-Iturbe, I., and J. M. Mejia, 1974: On the transformation of point rainfall to areal rainfall. *Water Resour. Res.,* **10,** 729–735.

Ryzhkov, A., D. Zrnić, and R. Fulton, 2000: Areal rainfall estimates using differential phase. *J. Appl. Meteor.,* **39,** 263–268.

Seed, A., and G. L. Austin, 1990: Variability of summer Florida rainfall and its significance for the estimation of rainfall by gages, radar, and satellite. *J. Geophys. Res.,* **95** (D3), 2207–2215.

Shimizu, K., 1993: A bivariate lognormal distribution with an analysis of rainfall data. *J. Appl. Meteor.,* **32,** 161–171.

Smith, J. A., and W. F. Krajewski, 1991: Estimation of the mean field bias of radar rainfall estimates. *J. Appl. Meteor.,* **30,** 397–412.

——, and ——, 1993: A modeling study of rainfall rate–reflectivity relationships. *Water Resour. Res.,* **29,** 2505–2514.

Stol, P. T., 1972: The relative efficiency of the density of rain-gage networks. *J. Hydrol.,* **15,** 193–208.

Tustison, B., E. Foufoula-Georgiou, and D. Harris, 2003: Scale-recursive estimation for multisensor quantitative precipitation forecast verification: A preliminary assessment. *J. Geophys. Res.,* **108,** 8377, doi:10.1029/2001JD001073.

Valdes, J. B., E. Ha, C. Yoo, and G. R. North, 1994: Stochastic characterization of space–time precipitation: Implications for remote sensing. *Adv. Water Res.,* **17,** 47–59.

Vanmarcke, E., 1983: *Random Fields: Analysis and Synthesis.* MIT Press, 382 pp.

Winchell, M., H. V. Gupta, and S. Sorooshian, 1998: On the simulation of infiltration- and saturation-excesses runoff using radar-based rainfall estimates: Effects of algorithm uncertainty and pixel aggregation. *Water Resour. Res.,* **34,** 2655–2670.

Yoo, C., J. B. Valdes, and G. R. North, 1996: Stochastic modeling of multidimensional precipitation fields considering spectral structure. *Water Resour. Res.,* **32,** 2175–2187.

Zawadzki, I. I., 1973: Statistical properties of precipitation patterns. *J. Appl. Meteor.,* **12,** 459–472.